JOURNAL OF AIRCRAFT
Vol. 31, No. 4, July–Aug. 1994

Side Force Augmentation at High Angle of Attack from Pneumatic Vortex Control

Kenneth C. Cornelius* and Gerald A. Lucius†
Wright State University, Dayton, Ohio 45435

An experiment has been undertaken to measure side and lift forces with various nozzle blowing locations on an elliptic forebody. In this study a jet of small momentum excites a convective instability to produce an amplified side force at high angle of attack for a fighter forebody. This study has identified an optimized nozzle position around the circumference of the forebody and axial location using a slotted nozzle at various pressure ratio values. A forward sweep of the nozzle provided for the greatest augmentation of side force at angles of attack below 55 deg. A beveled nozzle has shown active control of side force beyond 55-deg angle of attack and has merit in extending the angle of attack range. The mass flow requirements to produce a side force are sensitive to the angle of the jet relative to the forebody axis. The required mass flow is compatible with available engine bleed air that could be dedicated to pneumatic control. Data for different forebody strake configurations shows a degradation in side force magnitude with pneumatic blowing.

Nomenclature

A_{ref} = forebody reference area, 165 cm^2
C_l = lift coefficient, body axis
C_y = side force coefficient, body axis
C_μ = $(\dot{m}V_j/QA_{\text{ref}})$, $C_{\mu l}$ left nozzle blowing coefficient
D = nozzle diameter
D_e = equivalent forebody diameter, 14.5 cm
F = force
H = total head
L = total length of model, 36.8 cm
M = Mach number
M_m = moment
$\dot{m}$ = nozzle mass flow rate
P = static pressure
P_r = pressure ratio, nozzle plenum total/tunnel static
P_0 = total pressure
Q = dynamic head
R_l = Reynolds number based on forebody length, 6.1×10^5
$(U, V, W)_t$ = mean velocity, tunnel coordinates
V_j = jet exit velocity
$(X, Y, Z)_m$ = coordinate axis, model coordinates
α = angle of attack
β = sideslip angle
θ = nozzle sweep angle
ξ_n = normalized vorticity $\xi_x D_e/U_\infty$

Introduction

FUTURE air combat will require aircraft maneuver performance that will exceed the capability of present day fighters. At high angles of attack in the poststall region, the aerodynamic control surfaces such as the vertical tail and rudder become engulfed in the separated flowfield of the wing and lose their ability to impart the yawing moment and side force required for active control of the vehicle. Compounding this problem further, the aircraft is susceptible to asymmetrical side forces generated in the vicinity of the apex of the fuselage or nose when the vehicle's angle of attack is beyond 30–50 deg. These forces are due to the bistable nature of the three-dimensional boundary-layer separation around the periphery of the nose causing unequal strength vortical separations around the forebody. The resulting flowfield may lead to an unstable side force and yawing moment which are detrimental to the controlled motion of the aircraft. This lateral instability must be rectified if poststall multiaxes maneuvering of fighter aircraft is to become a realistic goal.

The key technology that is needed is the extension of aerodynamic control in the poststall regime of the flight envelope. A most promising approach for enhanced dynamic control of the aircraft is the use of properly placed blowing pneumatic jets in the nose region of the forebody which alters the bistable nature of the asymmetrical development of the vortical separations. This would allow controlled side force and yawing moments to be activated by the variation of the jet momentum. The stability of the vortex flow in the nose region is increased by the use of low aspect ratio strakes on the side of the forebody nose. The vortices generated from the strakes interact with the shed vorticity from the sides of the forebody to provide greater aerodynamic stability throughout an expanded operational flight regime. However, the extension of the flight envelope to higher angles of attack and the increase of the stall-spin resistance may be limited by the onset of vortex breakdown from either of the individual vortex formations and its interaction with the aircraft control surfaces.

Roll agility in modern fighters is often limited by the onset of lateral-directional instability which can be governed by the bistable vortex separation around the periphery of the aircraft nose. By blowing tangentially to the forebody surface on the leeward side of the vortex in the nose region, various investigators[1–8] have demonstrated significant control and aerodynamic enhancement of maneuverability. A critical review and bibliography of this technology is available.[9] Both yaw and side force control at high angles of attack can be enhanced by controlling the forebody vortex separation position and strength around the periphery of the nose. With precise control of forebody vortex aerodynamics the potential exists to minimize the required tail surface and improve the maneuver envelope of fighter aircraft. Previous results[6,7] on the X-29 forebody showed an increase in the side force magnitude the closer the nozzle was positioned to the apex of the

---

Received Jan. 19, 1993; presented as Paper 93-2959 at the AIAA 24th Fluid Dynamics Conference, Orlando, FL, July 6–9, 1993; revision received Aug. 2, 1993; accepted for publication Aug. 2, 1993.

*Assistant Professor, Department of Mechanical and Materials Engineering.

†Graduate Student. Member AIAA.

forebody. For the X-29 study the nozzle placement was fixed at two axial locations and a fixed peripheral position of 45 deg from the horizontal centerline of the forebody. The question of the optimum nozzle placement for maximum side force was only partially examined.

The experimental procedure outlined in the current study explored the impact of altering the forebody vortical separation lines along the fuselage with the desired goal of producing the maximum yawing moment and side force. The experimental goal was to determine the angle of the jet and nozzle placement on the forebody which would amplify the favorable jet/vortical interaction with the local aerodynamic forebody surface. If the required mass flow rates are in the range of conventional bleed air from the engine, then pneumatics become a viable option for forebody vortex control.

Model Construction

The details of the forebody model configuration used for the study are shown in Fig. 1. The model is an elliptic nose forebody. It was constructed from fiberglass and has a length of 36.8 cm, a maximum width of 16.25 cm, and a height of 12.9 cm with elliptical cross sections throughout the length. It was fastened to a rear plate which was machined to accommodate an internal balance. Two nozzle blocks were machined separately and mated with the internal surface of the model at a number of axial positions from the nose apex and placed asymmetrically about the centerline. Figure 2 shows a top view of the forebody with nozzles installed in the third axial location. O-rings were integrally designed in the nozzle blocks so that each nozzle could be rotated to the desired angle without leakage of the compressed air. The cross-sectional area at the rear of the forebody is 165.0 cm^2 with an effective diameter of 14.5 cm which correlates to a nondimensional length $L/D_e = 2.54$. The rear of the model had an aluminum support plate which was machined symmetrical about the model centerline to accommodate the model support sting and the flexible air lines. The nozzle blocks were integrally connected to the inside surface. The individual nozzles were designed to screw into the nozzle blocks, and the exit plane was configured to be normal to the local surface of curvature of the model at the various axial locations. Nozzle plugs were installed in adjacent ports so that blowing could be exercised from one port at a time. The model support sting was integrally connected to the internal force balance and the flexible pressure lines were placed symmetrically to the sting to supply compressed air to either side of the nozzle blocks. Induced loads from pressurizing the pneumatic lines with no mass flow resulted in a maximum tear correction of 1.2/granular glass beads of width 0.5 cm placed on the sides of the forebody to activate transition to a turbulent boundary layer. The nose boom in front of the forebody was attached for all the forebody force data.

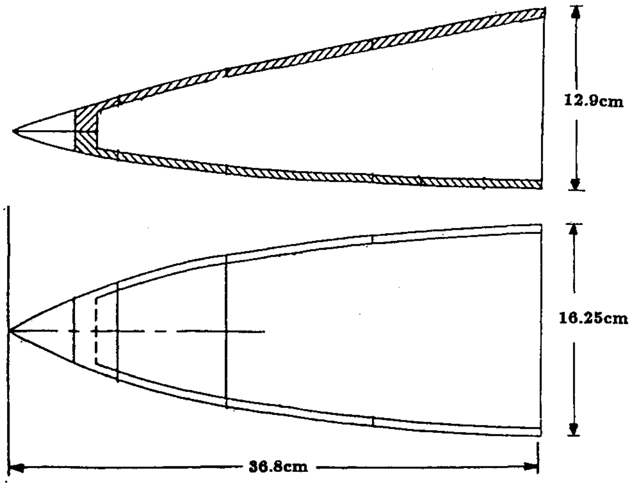

Fig. 1 Forebody model configuration.

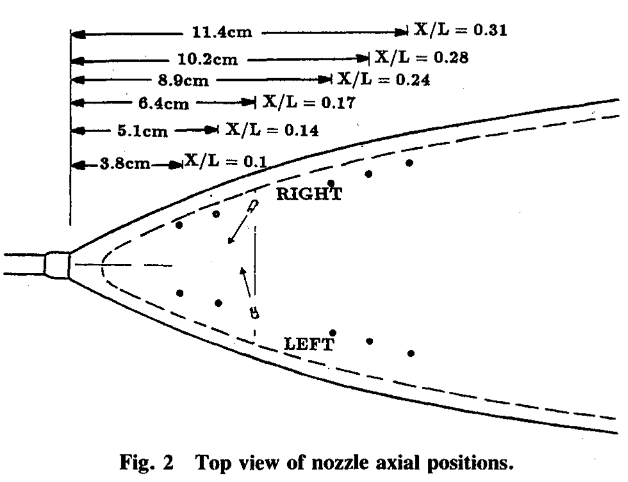

Fig. 2 Top view of nozzle axial positions.

Test Facility

The test was conducted in the Low Speed Wind Tunnel at Wright State University. The tunnel is fully instrumented and principally dedicated for force measurements about aerodynamic configurations. The tunnel used in this investigation is a open-return pressure wind tunnel powered by a 20-hp motor attached to an axial flow fan. The test section size is 0.61 m high, 0.61 m wide, and 1.22 m in length. The maximum speed utilized in this test was 25 m/s. The freestream speed is controlled by monitoring a set of calibrated Piezzio rings installed upstream of the test section. The model was mounted onto a long sting to facilitate two degrees of freedom (DOF) for the pitch and sideslip axis. The mass flow was determined by a set of calibrated venturies in series with two pressure lines connected to the nozzle blocks. A Plexiglas® sidewall of the test section provides for optical transmission for flow visualization using dye.

Nozzle Placement and Exit Geometry

Nozzle Placement on Forebody

Prior to fixing the nozzle positions on the forebody a preliminary test was undertaken to find the best location of the nozzle around the periphery for the maximum side force. The jet was attached to an external three-dimensional traverse for positioning the jet one diameter from the surface in a nonmetric configuration and blowing at various locations while measuring the side force for each position. The nozzle exit plane could be adjusted manually in pitch and yaw through a connection which allowed two DOF. The nozzle exit plane was bent at 90 deg to an extended tube of length 20 cm to minimize the flow interference. From this preliminary test the nozzle blocks were positioned to accommodate two angles around the periphery of the forebody. The nozzle exit plane was configured to be 20 and 30 deg, respectively, for the left

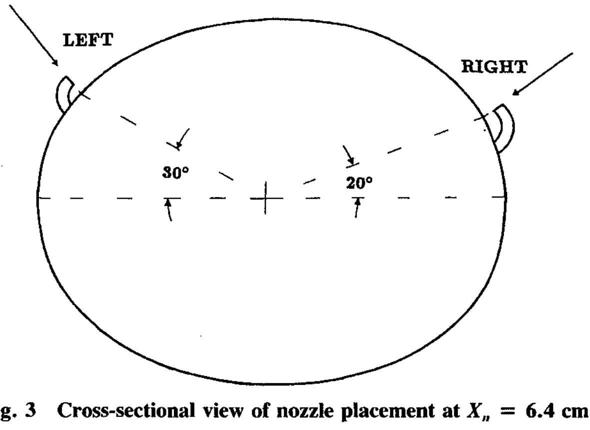

Fig. 3 Cross-sectional view of nozzle placement at X_n = 6.4 cm.

and right nozzles, as shown in Fig. 3. The nozzle position was measured from the horizontal line bisecting the model midway between the top and bottom of the forebody cross section. The nozzle exit plane was positioned a minimum of one diameter from the surface of the model and perpendicular to the forebody surface curvature. Positioning the nozzles around the apex of the nose at two separate angles allowed an independent check on this parameter.

Slotted Nozzle S1

It was postulated[6] that greater entrainment in the near field would result in greater asymmetry in the forebody vortex flowfield. This reasoning led to the optimized nozzle S1 shown in Fig. 4 with an axisymmetric contraction at the base with an extended throat region. A slot was then milled on adjacent sides of the throat region to allow the Prandtl-Meyer expansion of the flow to occur in two dimension. The nozzles had a radius of curvature of 2.5 times the i.d. which turned the jet flow 90 deg from the contoured contraction at the base of the nozzle. This configuration allowed the jet to expand supersonically into a two-dimensional sheet which provided for greater aerodynamic interaction between the expanding jet flow and the flowfield about the forebody.

The basic physics of the expansion is shown in Fig. 5. The spread angle can be estimated from the two-dimensional theory of the Prandtl-Meyer expansion of the outer streamline[10] which is defined by the shear layer as it expands to atmospheric pressure. This geometry allows the flow to be self-adjusting, i.e., the spread angle increases with increasing P_r. The reflected compressive waves reconverge in the center portion of the flow with local oblique expansion and compressive waves. The outer flow escapes the reflected compressive wave reconvergence due to the three-dimensional nature of the supersonic expansion. A laser light sheet using small seed particles as the scattering media produced a cross-sectional view of the boundary of the jet. Figure 6 shows the photograph comparison, when viewed down the x axis, of an axisymmetric nozzle flow to the slotted nozzle flowfield at the downstream location of X/D = 12 and 24 with P_r = 7.5. Using this qualitative optical technique the flow structure which emanates from the slotted nozzle has greater entrainment by virtue of the vortex dynamics.

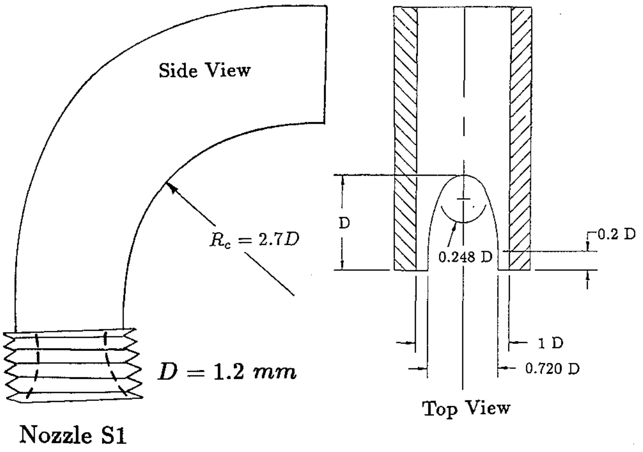

Fig. 4 Sketch of nozzle S1, dimensions are normalized on D = 1.2 mm.

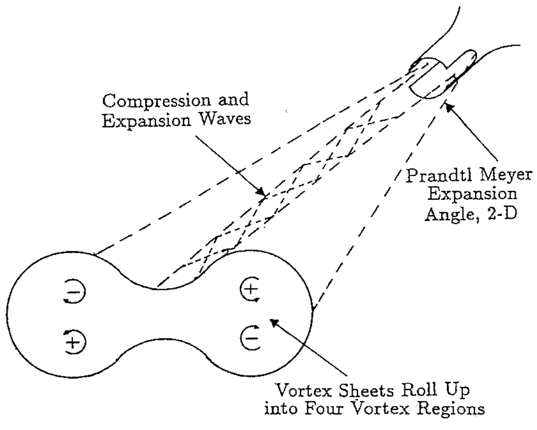

Fig. 5 Physics of supersonic expansion of slotted nozzle S1.

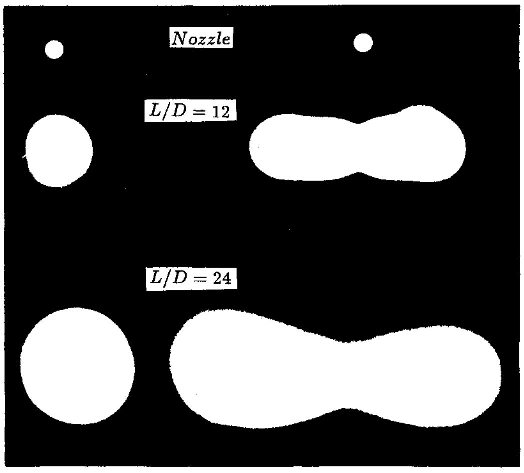

Fig. 6 Photograph of light sheet at P_r = 7.3 of jet cross section.

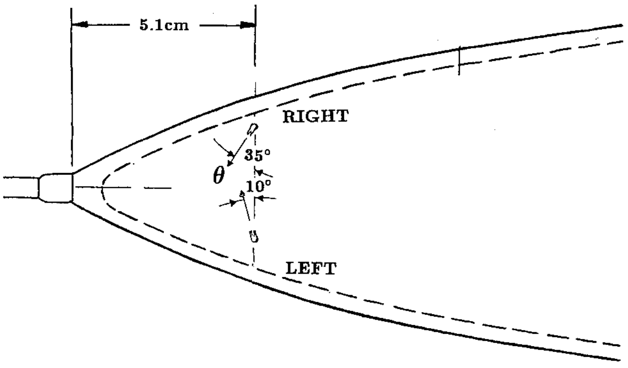

Fig. 7 Configuration for maximum effect on side force no strakes.

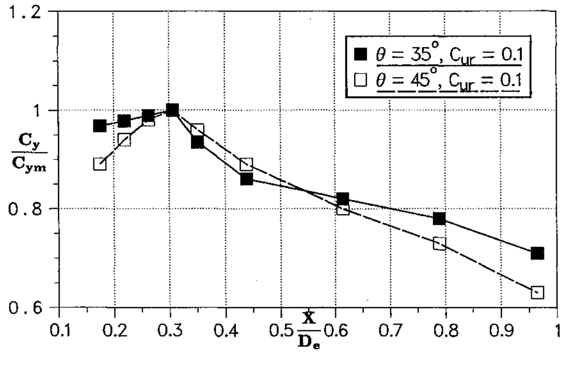

Fig. 8 Side force coefficient vs X/D_e, $C_{\mu r}$ = 0.1, θ = 35 deg, α = 45 deg.

Experimental Results

Comparison of Exit Nozzle Diameter at Various P_r Values

Different nozzle exit diameters of the slotted nozzle S1 with an i.d. from 0.84–1.42 mm were investigated with the nozzle yawing vector at the optimum pointing angle. The nozzles were individually inserted into the nozzle plenum at a fixed axial location. Figure 7 shows the nozzle position and configuration for maximum effect on side force with no forebody strakes. The nozzles had their greatest effect on the side force with a 35-deg forward yaw angle for the right nozzle, and a

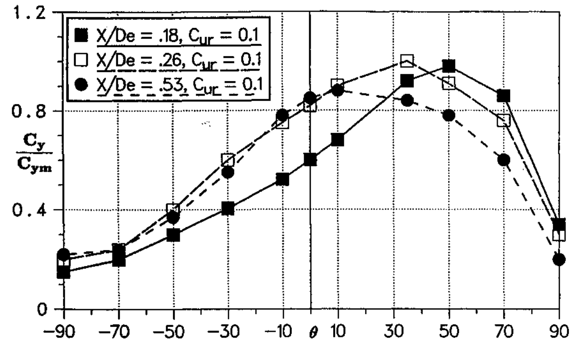

Fig. 9 Side force coefficient vs nozzle sweep angle at various axial positions with $C_{\mu r} = 0.1$, α = 45 deg.

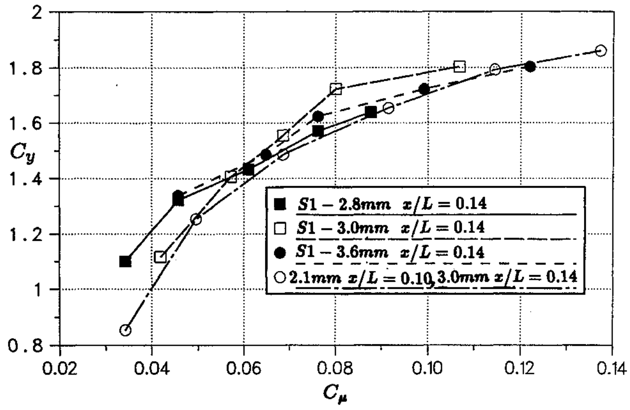

Fig. 10 Side force coefficient vs C_μ at X_n = 5.1 cm, α = 45 deg.

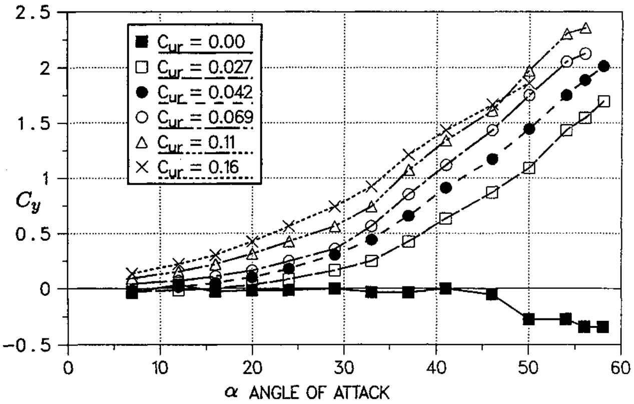

Fig. 11 Side force coefficient vs α for various C_μ at X_n = 5.1 cm.

10-deg yaw for the left nozzle where the nozzle yaw angle was measured from the perpendicular line to the body axis. A positive value of θ represents a forward sweep of the nozzles as shown in Fig. 7. Figure 8 is a plot of the side force coefficient normalized on the maximum value vs different nozzle axial locations X/D_e. The nozzle blowing coefficient was maintained at $C_{\mu r}$ = 0.1, with a nozzle sweep angle of θ = 35 deg, and forebody angle of attack of α = 45 deg. Figure 9 is a plot of side force coefficient normalized on the maximum value vs nozzle sweep angle at different axial locations, with $C_{\mu r}$ = 0.1 and forebody angle of attack of α = 45 deg. Blowing from the left nozzle the data exhibited similar trends.

Figure 10 shows the side force coefficient vs C_μ at the nozzle position of X = 5.1 cm with α = 45 deg. Different nozzle diameters were used in this data set with a corresponding higher P_r for equivalent C_μ. No significant change in magnitude of the side force was noted by increasing the P_r while maintaining C_μ as constant, although the maximum P_r attainable from the compressed air line was 7.5 for this data. Figure 11 shows the side force coefficient vs α for various $C_{\mu r}$ blowing from the right nozzle. A significant change in slope is apparent

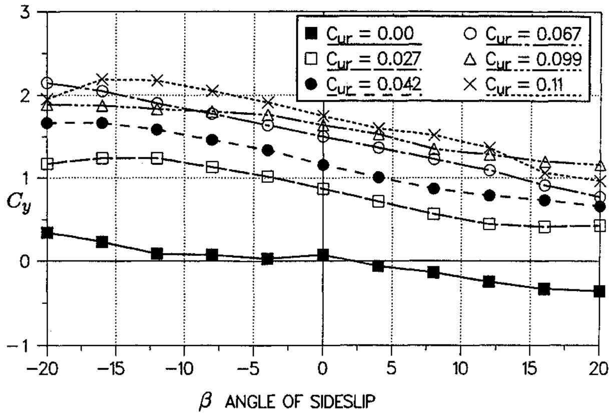

Fig. 12 Side force vs sideslip angle various C_μ at X_n = 5.1 cm, α = 45 deg.

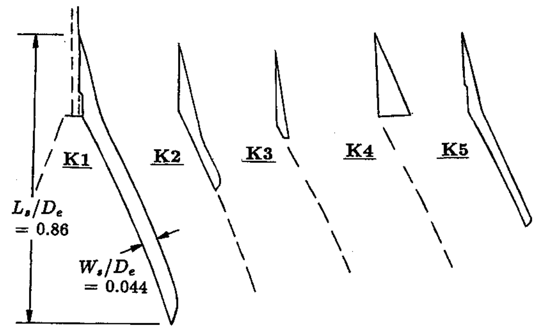

Fig. 13 Forebody strake configurations.

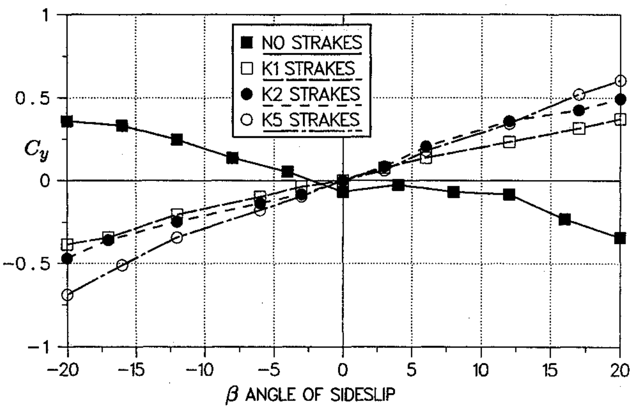

Fig. 14 No blowing sideslip characteristics with strakes K1, K2, K5, α = 45 deg.

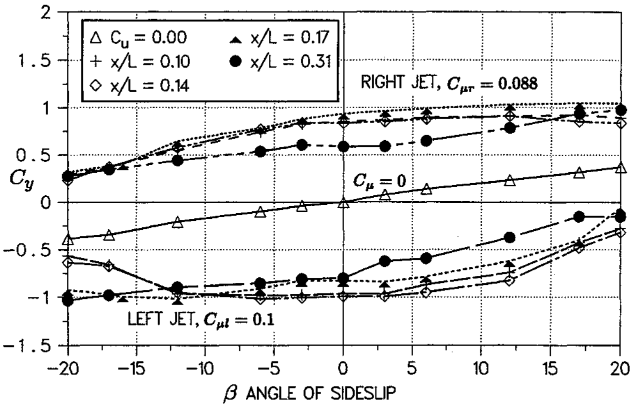

Fig. 15 Variation of nozzle axial location on sideslip characteristics with K1 strake α = 45 deg.

beyond $\alpha = 30$ deg with greater amplification of the side force. Figure 12 shows the side force vs sideslip angle for various C_μ at $X = 5.1$ cm and $\alpha = 45$ deg. The data for the nozzle position at $X = 5.1$ cm were superior to a nozzle positioned forward of this location. A greater range of C_μ vs side force was attainable, and side force characteristics were maintained for larger side slip angles. When the nozzle was positioned at $X = 3.8$ cm at a 10-deg sideslip angle the model began to shake due to a time-dependent, low-frequency shedding of the vorticity.

Forebody Strake Data

Nose strakes have been used in the past to overcome the bistable nature of the vortex asymmetric orientation at the nose of the forebody. The strakes offer a stabilizing influence at zero yaw at higher angles of attack. This section describes the influence of the strake configurations on the side force augmentation by blowing. Figure 13 shows the geometry of the forebody strake configurations labeled (K1–K5). Figure 14 shows the no blowing sideslip characteristics with strakes K1, K2, and K5. These strake configurations demonstrate an equivalent magnitude change in slope for the side force vs the sideslip angle. The addition of strakes provides lateral (directional) static stability, as compared to the forebody without strakes which is statically unstable. The pitot strakes (K3, K4) which extend in front of the forebody change the slope of the curve over a limited sideslip range. Figure 15 shows the side force coefficient magnitude vs sideslip characteristics with variation of nozzle axial location with the forebody K1 strakes. The reduction in magnitude of a factor of 2 on the side force coefficient in comparison to the no strake configuration suggests that smaller strakes would have less of an impact on the blowing effectiveness.

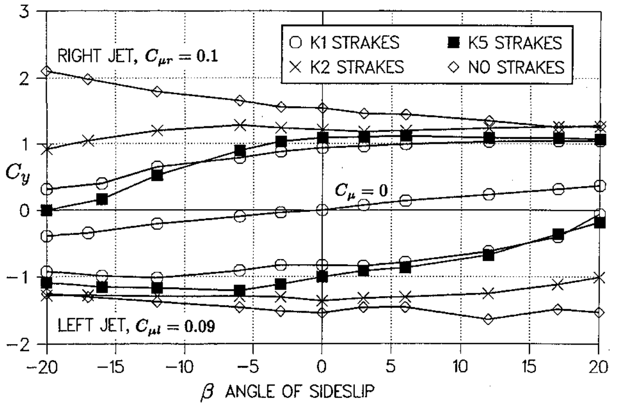

Fig. 16 Different strake comparison with blowing at $X_n = 6.4$ cm, $\alpha = 45$ deg.

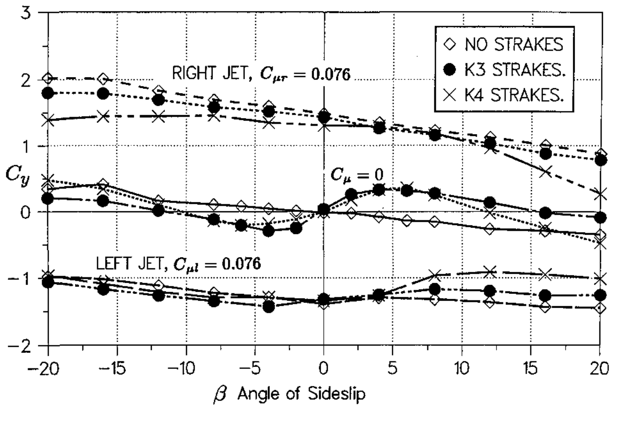

Fig. 17 Sideslip characteristics with smaller strakes $\alpha = 45$ deg.

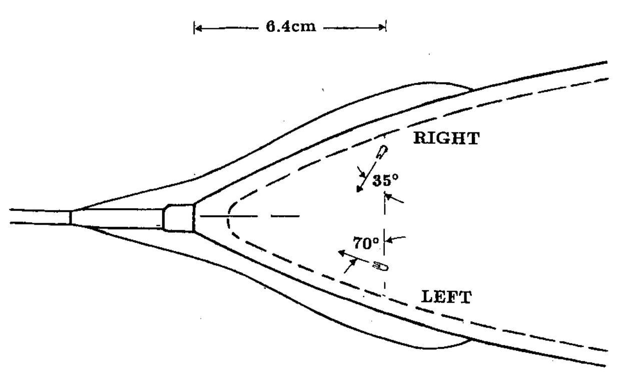

Fig. 18 Configuration for maximum effect on side force with K1 strake.

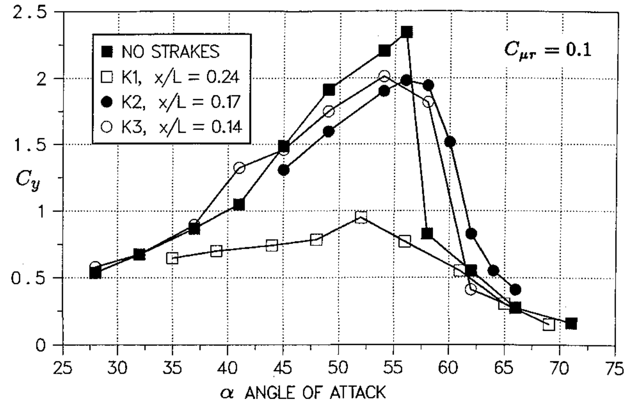

Fig. 19 Side force coefficient vs α for various strake configurations $C_{\mu r} = 0.1$.

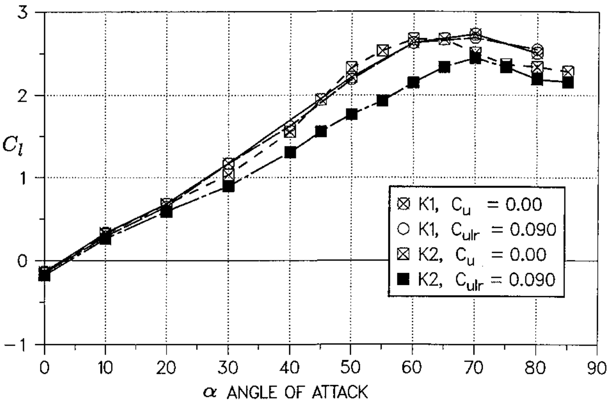

Fig. 20 Lift force coefficient vs α no blowing.

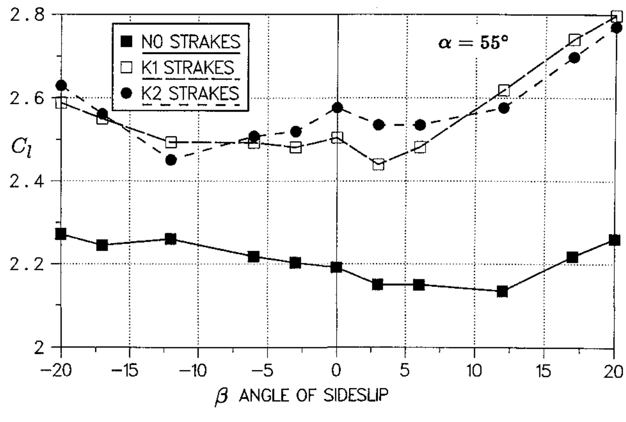

Fig. 21 Lift force coefficient vs sideslip angle no blowing $\alpha = 55$ deg.

Figure 16 shows the different strake comparisons while blowing at $X = 6.4$ cm. Figure 17 demonstrates that forebody blowing with the smaller strakes gives less reduction in blow-

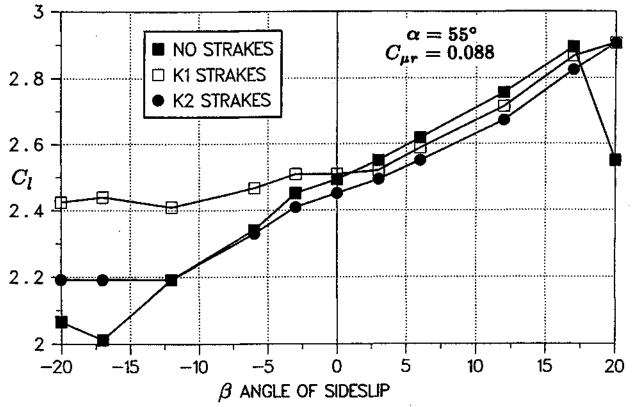

Fig. 22 Lift force coefficient vs sideslip angle $C_{\mu r} = 0.088$, $\alpha = 55$ deg.

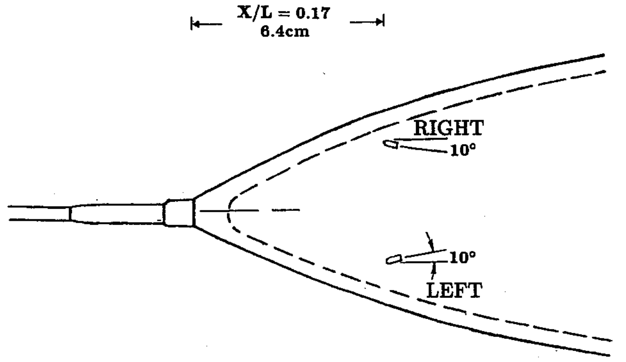

Fig. 23 Configuration for maximum effect on side force with nozzle F1.

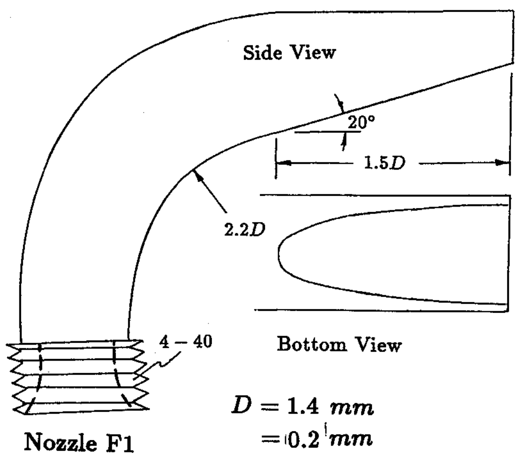

Fig. 24 Side view of nozzle F1.

ing effectiveness, while retaining the lateral static stability. Since the separation line is fixed with the strake forebody combination, the amplification from blowing is diminished as compared to the clean forebody. Figure 18 shows the configuration for maximum effect on the side force with the K1 strake. Figure 19 shows the side force coefficient vs α for various C_μ values with the baseline strake K1 and the smaller strakes. The amplification reduction with the larger strakes is apparent throughout the angle-of-attack range.

Forebody Lift Force

Figure 20 shows the lift force coefficient vs α with no blowing. The lift force increases on the forebody up to a 60-deg angle of attack with a moderate stall characteristic at higher angles. This tendency increases the nose-up pitching moment for the aircraft. Figure 21 shows the lift force coefficient vs sideslip angle where the straked configuration shows higher

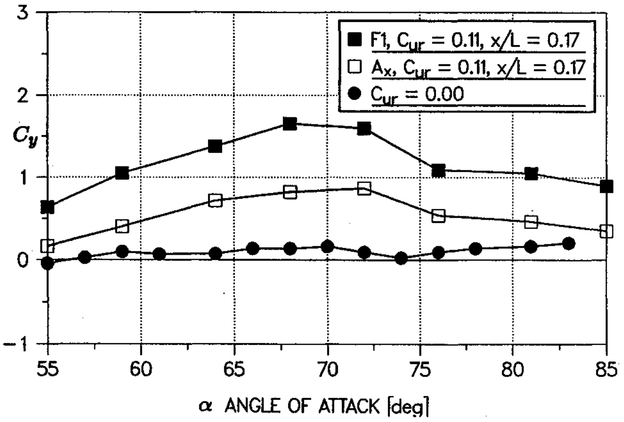

Fig. 25 Side force coefficient vs α at $C_{\mu r} = 0.11$.

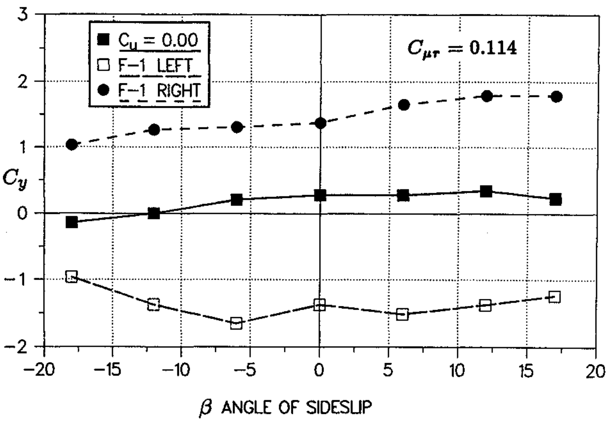

Fig. 26 Side force coefficient vs sideslip angle at $\alpha = 70$ deg, $C_{\mu r} = 0.114$.

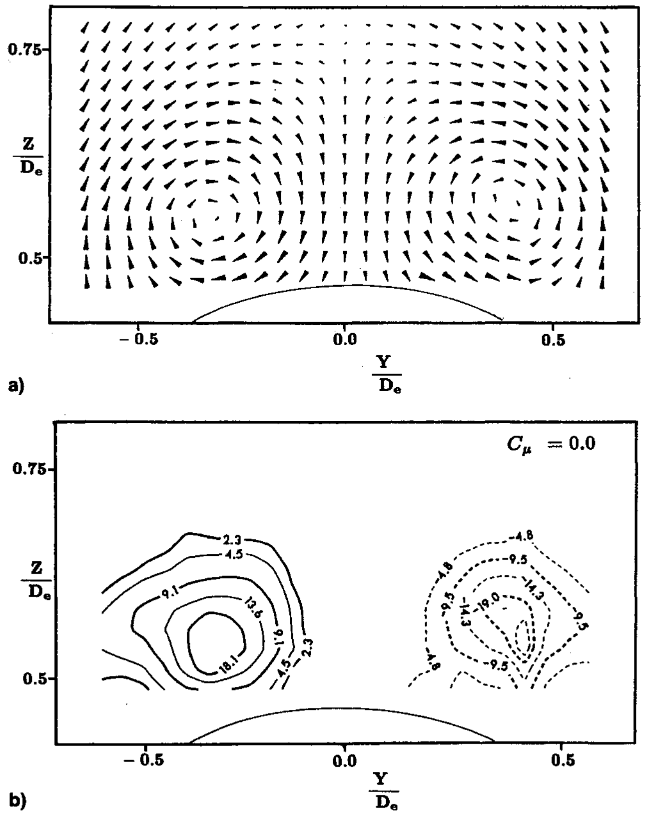

Fig. 27 a) Crossflow vector plot at $\alpha = 45$ deg and b) vorticity $2\xi_n$ contours at $\alpha = 45$ deg, $C_\mu = 0.0$.

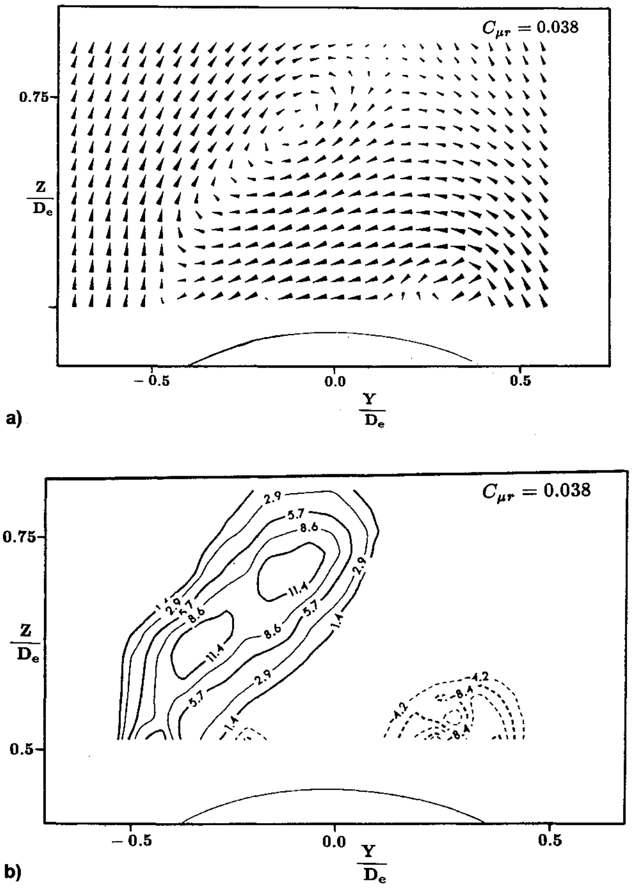

Fig. 28 a) Crossflow vector plot at $\alpha = 45$ deg, $C_{\mu r} = 0.038$ and b) vorticity $2\xi_n$ contours at $\alpha = 45$ deg, $C_{\mu r} = 0.038$.

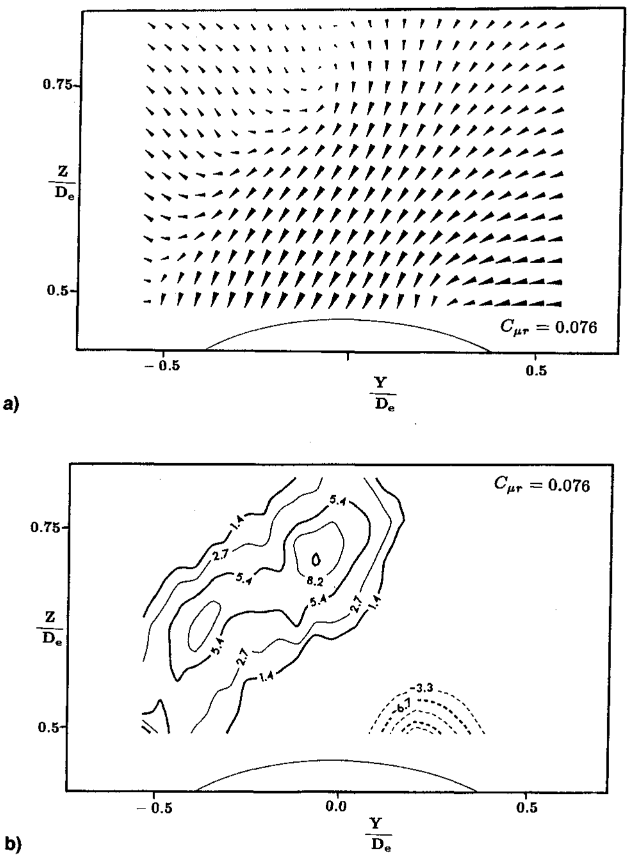

Fig. 29 a) Crossflow vector plot at $\alpha = 45$ deg, $C_{\mu r} = 0.076$ and b) vorticity $2\xi_n$ contours at $\alpha = 45$ deg, $C_{\mu r} = 0.076$.

lift forces. Figure 22 shows the lift force coefficient vs sideslip angle while blowing on the right nozzle with $C_\mu = 0.088$. The lift force increases above the no blowing baseline data when the model is sideslipped to a $+\beta$ while blowing from the right nozzle.

High Angle of Attack with F1 Beveled Nozzle

Figure 23 shows the nozzle configuration for maximum effect on the side force with the nozzle placed at $X = 6.4$ cm. The blowing angle is directed down the axis of the model with an inboard yaw of 10 deg from the longitudinal axis of the model. Figure 24 shows a sketch of the side view of the beveled nozzle F1. The nozzle geometry was designed with a 20-deg beveled cut at the end of the nozzle which provides for an asymmetric expansion allowing the resultant jet angle to be vectored toward the surface of the model. The jet impinges on the forebody surface and spreads out laterally, acting as a boundary-layer control jet. The magnitude of the side force was found to be 70% greater with nozzle F1 as compared to the equivalent blowing in the same direction from the slotted S1 or axisymmetric nozzle. The magnitude of the side force was sensitive to the nozzle sweep angle from the body axis, with a 10-deg change reducing the magnitude of the side force by 50%. Figure 25 shows the side force coefficient vs α beyond a 55-deg angle of attack at $C_\mu = 0.114$ for both the F1 and axisymmetric nozzle with no strakes on the forebody. Figure 26 shows the side force coefficient vs sideslip angle at $\alpha = 70$ deg, $C_\mu = 0.114$. The physics of producing a side force with jet blowing with nozzle F1 at a high angle of attack is attributed to controlling the vortex strength on the blowing side by preventing the departure or separation of the vortex flow from the forebody surface.

7-Hole Probe Measurements

Wake traverses of 7-hole probe measurements allowed the three-dimensional velocity to be calculated in the near wake to quantify the flow interaction with and without blowing. The probe was mounted on a computer controlled three-dimensional traverse and the measurements were obtained at an axial distance of 2.0 cm behind the base of the model. The vorticity was calculated using Stokes theorem utilizing the measured velocity at four adjacent grid points. The data acquired was for the unstraked forebody with the optimized nozzle S-1. At an angle of attack of $\alpha = 45$ deg, the forebody flow exhibits two symmetrical vortices in the (y, z) plane in the near wake. The vortex flow remains attached to the forebody and is responsible for the vortex lift on the nose section and the corresponding nose-up pitching moment. Figures 27a and 27b show the (V, W) vectors and the corresponding vorticity values at $\alpha = 45$ deg for no blowing. Figures 28a and 28b show the (V, W) vectors and the resultant vorticity values at $\alpha = 45$ deg while blowing from the right nozzle at $C_\mu = 0.038$. Figures 29a and 29b show the (V, W) vectors and the corresponding vorticity values at $\alpha = 45$ deg and blowing from the right nozzle at $C_\mu = 0.076$. The wake surveys downstream from the forebody model show the basic interaction of the jets with the separated vortex flow. At low blowing rates from the nozzle, the vorticity contours of the separated flowfield demonstrate that blowing across the body results in a reduction of the vortex strength on the blowing side while the flow remains nearly attached. The opposite side vortex is pushed away from the body and the jet/crossflow vorticity merges with the vortex sheet from the separated flow on the opposite side. This twofold flow interaction is responsible for the augmentation in the side force.

Conclusions

A parametric study examined the placement of a nozzle both axially and circumferentially to maximize the side force for a fixed blowing rate. This research has identified jet nozzle configurations which directly influence the position and strength of the separated vortex flow to enhance the jet/vortical interactions favorably. The mass flow requirements for an equivalent yawing moment are sensitive to the angle of the jet momentum and placement on the forebody. Significant amplification of the side force occurs when the jet is yawed with a forward sweep. The following conclusions are drawn from this study:

1) Maximum augmentation of the side force is achieved by orienting the slotted S1 nozzle at a forward sweep of (10–35 deg) from the perpendicular to the model axis and located at a peripheral forebody angle of (20–30 deg).

2) Forebody with no strakes has demonstrated greater amplification of the side force at low blowing rates with the greatest augmentation at $C_\mu \leq 0.095$ and a nozzle axial location of $X/D_e = 0.35$.

3) At a high angle of attack a beveled nozzle F1 placed at $X/D_e = 0.44$ and oriented at a sweep of (10–15 deg) inboard from the model axis at a peripheral forebody angle of (20–30 deg) shows a significant augmentation of the side force at $\alpha \geq 55$ deg.

4) The straked forebody exhibits lateral static stability with a sideslip angle with different size strakes.

5) With a straked forebody, as the strake length increases the blowing effectiveness decreases due to the fixed separation line. The smaller length strakes are recommended since there is less impact on the side force amplification by blowing. The optimum axial location for the nozzle placement is $X/D_e = 0.44$.

The ramifications of altering the vortex flow pattern are apparent from these results. A pneumatic jet placed in the nose region and rotated with a forward sweep has the following favorable characteristics in terms of amplifying the side force for a fixed blowing coefficient. A nozzle S1 which undergoes a supersonic expansion in the vertical plane and is yawed 120 deg to the forebody axis shows the greatest sensitivity in augmenting the yawing moment for a fixed blowing coefficient. By blowing across the forebody the vortex flow adjacent to the blowing jet becomes stabilized, moving the separation line further around the fuselage. The jet/crossflow interaction across the centerline of the model pushes the adjacent vortical core away from the surface, producing a twofold effect on the asymmetry.

Acknowledgments

This research was funded under Contract F33601-89-D0045 from the Flight Dynamics Laboratory, Wright Patterson Air Force Base, Ohio. The authors would like to acknowledge the helpful discussions with Russ Osborne, B. Guyton, and S. LeMay from the Aeromechanics Division.

References

[1] Skow, A. M., Titiriga, A., and Moore, W. A., "Forebody/Wing Vortex Interactions and Their Influence on Departure and Spin Resistance," High Angle of Attack Aerodynamics, AGARD CP-247, Oct. 1978.

[2] Skow, A. M., and Peake, D. J., "Control of the Forebody Vortex Orientation by Asymmetric Air Injection," AGARD CP-262-15, May 1979.

[3] Peake, D. J., Owen, F. K., and Johnson, D. A., "Control of Forebody Vortex Orientation to Alleviate Side Forces," AIAA Paper 80-0183, Jan. 1980.

[4] Guyton, R. W., Osborn, R. F., and LeMay, S. P., "Forebody Vortex Control Aeromechanics," AGARD Fluid Dynamics Panel, Paper 16, Toulouse, France, May 1991.

[5] Malcomb, G. N., Ng, T. T., Lewis, L. C., and Murri, D. G., "Development of Nonconventional Control Methods for High Angle of Attack Flight Using Vortex Manipulation," AIAA Paper 89-2192, 1989.

[6] Cornelius, K. C., Pandit, N., Osborne R. F., and Guyton R. W., "Experimental Study of Pneumatic Control of Forebody Vortices at High Alpha," *Journal of Aircraft*, Vol. 31, No. 1, 1994, pp. 49–56.

[7] Guyton, R. W., and Maerki, G., "X-29 Forebody Jet Blowing," AIAA Paper 92-0017, Jan. 1992.

[8] LeMay, S. P., Sewall, W. G., and Henderson, J. F., "Forebody Vortex Flow Control on the F-16C Using Tangential Slot and Jet Nozzle Blowing," AIAA Paper 92-0019, Jan. 1992.

[9] Ericsson, L. E., "Control of Forebody Flow Asymmetry, a Critical Review," AIAA Paper 90-2833, Sept. 1990.

[10] Shapiro, A. H., *The Dynamics and Thermodynamics of Compressible Fluid Flow*, Vol. 1, Wiley, New York, 1953, pp. 450–490.